Homemade 3-carbon electrode system for electrochemical sensing: Application to microRNA detection

Mariana C.C.G. Carneiro [a,b], Felismina T.C. Moreira [a], Rosa A.F. Dutra [c], Rúben Fernandes [b,d], M. Goreti F. Sales [a,*]

[a] BioMark-CINTESIS/ISEP, School of Engineering, Polytechnic Institute of Porto, Portugal
[b] School of Health, Polytechnic Institute of Porto, Portugal
[c] Biomedical Engineering Laboratory, Federal University of Pernambuco, Recife, Brazil
[d] Instituto de Investigação e Inovação em Saúde (i3S), University of Porto, Portugal

* Corresponding author at: School of Engineering of the Polytechnique School of Porto, R. Dr. António Bernardino de Almeida, 431, 4249-072 Porto, Portugal.
E-mail address: mgf@isep.ipp.pt (M.G.F. Sales).

A B S T R A C T

The homemade production of carbon screen-printed electrodes (C-SPEs) with a three carbon electrode system is reported, along with its application in electrochemical sensing. It is highlighted herein as main novelty that a simple carbon ink may be employed in the preparation of the 3-electrode system, including the pseudo-reference electrode, thereby avoiding the addition of silver or other suitable metal and simplify the construction of such devices, reducing costs and time.

Screen-printed technology was employed to produce the 3-electrodes and the corresponding electrical paths. This was achieved by the manual application of a commercial carbon ink into a polyvinyl chloride (PVC) substrate allowing the production of >20 SPEs. The optimization of the SPE assembly was made by univariate mode, until the best electrical features of the electrode-solution interface were achieved. Several electrochemical techniques were used for this purpose, namely cyclic voltammetry (CV), square wave voltammetry (SWV) and electrochemical impedance spectroscopy (EIS). Raman Spectroscopy and Thermogravimetric Analysis (TGA) were also used for materials and electrode surface characterization.

The usefulness of such devices was tested by modifying the working electrode with a sensing layer for microRNA-107, a potential biomarker in Alzheimer's Disease (AD). For this purpose, the surface was functionalized with carboxylic groups, activated by carbodiimide reaction and bound to a suitable oligonucleotide probe containing the complementary sequence. Finally, the microRNA-107 sequence hybridized with its probe, proving the efficiency of the C-SPEs in electrochemical sensing.

Overall, this study brings into light the possibility of preparing simple homemade electrodes with a 3 carbon electrode system that stands out by the low cost, disposability and versatility of the presented platform, holding a great potential for application in point-of-care devices using electrochemical sensing.

Keywords: Screen-printed electrodes 3 carbon electrodes Electrochemical biosensors Carbon-reference electrode microRNA-107 Alzheimer disease

1. Introduction

Conventional quantification of nucleic acids generally involves signal amplification steps, based on extensive protocols, that provides their ultrasensitive detection, lowing the limit of detection (LOD). In comparison with these conventional methods, electrochemistry has attracted substantial interest in nucleic acids analysis due to their advantages as low-cost, real-time and on-site detection [1].

Electrochemical biosensors gained increasing interest over the past decades, especially in the development of disposable point-of-care devices, in innumerous areas of application, as biomedical, industrial, pharmaceutical and environmental analyses [2,3]. Electrochemical biosensors sense the conversion of a biological response into an electrical measurable signal, proportional to the concentration of a given analyte in the sample to be analyzed [4]. These devices enable fast and real-time responses, linked to miniaturization and portability, low cost, simple procedures and a wide linear range, through the combination of the conventional molecular methods selectivity and the sensitivity related with the signal transduction [5]. Amperometry, potentiometry and conductimetry are the main electrochemical techniques employed in biosensor transduction [6].

Among the different electrodes employed in electrochemical biosensing, SPEs have been used in mass production of disposable low-cost electrodes for electrochemical detection and quantification of several compounds [4,5]. An SPE unit is typically a planar device combining 3-electrodes: working electrode (WE), reference electrode (RE) and auxiliary or counter electrode (AE/CE). These electrodes are produced by screen printing technology, through the layer-by-layer deposition

of an ink on a solid substrate [7,8]. Different substrates and a wide range of ink compositions have been used, depending of the final application.

Regarding substrates, the ink can be printed, for example, in plastic, alumina, ceramic, glass or polyethylene terephthalate. The ink is generally composed by an electrochemical active material (e.g. graphite), a polymeric binder (e.g. PVC, cellulose acetate, polyaniline, polyvinyl ferrocene acrylamide, phthalates, or silicon binder) to enhance the affinity of the ink for the subtract, and solvent(s) to improve the viscosity of the ink [9]. These polymeric binders generally lead to a slower electron transfer, which has been solved by the addition of electrocatalyst materials (e.g. noble metals, metal oxides) [2]. Carbon, silver and gold inks are the most popular materials, with carbon ink offering the advantage of low-cost and easy modification, along with chemical inertness and low background current [9]. Carbon-based inks based in graphite, graphene or carbon nanotubes are commonly used to produce the WE area [5,7]; gold and platinum are also employed. The CE may be produced by the same material as the WE, while the RE is mostly Ag-based [7].

Besides the substrate type and the ink composition, the selection of the mesh that defines the geometry and the size of the electrodes, the printing process and the drying and curing steps are also critical stages in SPEs construction, with significant influence in the electrochemical performance of the final electrodes [10]. In general, the WE has a circular shape and is surrounded by the CE and RE. The area of the CE is typically larger than that of the WE. The area of the RE is typically small and has not relation with the size of the other electrodes.

In addition to all these, after the SPE fabrication, a large range of materials are available for surface electrode modifications, such as metals, enzymes, polymers, nanomaterials, mediators or complexing agents [7,11–14]. These modifications can be made by incorporating different materials in the ink composition or by drop-casting a suspension with the nanomaterial and let the solvent evaporate at the electrode surface [2,7]. The use of nanomaterials in electrochemical sensing leads to an improvement in the performance of the devices. Carbon nanotubes (CNT) are the most common carbon-based nanomaterials employed, due to their excellent electrical and chemical properties, as well as their high surface-to-volume ratio, which increases the electrochemically-active area of the electrodes and accelerates electron transfer. CNTs can be easily modified, for example, through organic modifications with oxygen functional groups, biomolecules or polymers or by electrostatic interactions with suitable chemical functions. Overall, there is a great versatility of materials and flexibility in designing SPEs [7,11–14], and these devices are confined in a small area, allowing the reduce sample volumes to few microliters and achieving low LODs.

Facing the previous developments in the literature regarding SPEs, a breakthrough would be the use of carbon material also in the RE. The costs linked to the production process would decrease and the material would be stable for long periods, without specific storage requirements. In general, the typical Ag-based RE has stability issues and a conflicting problem with the presence of chloride [15] in the samples (a common species in biological fluids), which would not happen herein because the sample may be incubated only in the WE area.

Thus, this work reports the production of homemade SPEs with a 3 carbon electrode system, assembled on low-cost substrates by screen-printed technology. As far as we know, this is the first report in the literature where the 3-electrode system of SPEs is prepared with the same carbon ink. Herein, similar SPEs were prepared with a silver ink on the RE area, for comparison purposes. The main variables influencing the assembly strategy are optimized and the resulting electrical features given.

As proof-of-concept, the homemade SPEs are applied herein to detect microRNA-107. MicroRNAs are non-coding RNAs involved in post-transcriptional regulation of gene expression, having a major role in several processes, as neurodegeneration. The expression of microRNA-107 has been reported to be down regulated in temporal cortex [16,17] and in blood samples [18] of people with AD, at an early stage of the disease. So, this microRNA, involved in the regulation of several molecules related with AD pathophysiology [18], is a promising non-invasive biomarker for this disease, as it can be found in body fluids. Moreover, it has a potential application in early diagnosis, in alternative to the actual diagnostic methods which are invasive and expensive [16,17]. Conventional microRNA analysis includes northern blot, microarrays and quantitative real-time polymerase chain reaction (qRT-PCR), slow and expensive molecular techniques with several sources of bias and lack of reproducibility. Electrochemical detection of miRNAs emerges as a fast and low-cost method for quantitative analysis, with high selectivity and sensitivity [19,20], but as far as we know there is no biosensor described for the detection of miRNA-107. In general, a simple way to detect oligonucleotides is to use a complementary sequence on the intended receptor surface. There are several approaches towards electrochemical biosensing, but these involve mostly gold, either as an electrode support [21] or in a composite form that includes gold nanostructures [22].

Thus, this work presents the construction of C-SPEs on PVC supports and their preliminary testing in the detection of microRNA on a carbon support. The biosensor is assembled with an amine-oligonucleotide complementary probe and the microRNA is subsequently detected by hybridization, which changes the charge-transfer resistance of the electrode surface in the presence of a standard redox probe of iron.

2. Experimental

2.1. Reagents and solutions

All chemicals were analytical grade and ultrapure water was obtained from a Milli-Q water purification system. Potassium hexacyanoferrate II-3-hydrate ($K_4[Fe(CN)_6]$), potassium hexacyanoferrate III ($K_3[Fe(CN)_6]$), potassium nitrate (KNO_3) and disodium hydrogen phosphate ($Na_2HPO_4{\cdot}2H_2O$) were obtained from Riedel de Haën; potassium chloride (KCl) from Merck; phosphate buffered saline (PBS) tablets from Amresco; lithium perchlorate ($LiClO_4$) and multi-walled carbon nanotubes functionalized with carboxylic acid groups (MWCNTs-COOH), L-Aspargine ($C_4H_8N_2O_3$), diethyl pyrocarbonate (DEPC) 99% ($C_6H_{10}O_5$) and 4-(2-hydroxyethyl)-1-piperazineethanesulfonic acid (HEPES, $C_8H_{18}N_2O_4S$) from Sigma Aldrich; iron (III) chloride ($FeCl_3.6H_2O$) from Scharlau; *N*,*N*-Dimethylformamide (DMF) (C_3H_7NO) from Analar Normapur; 1-ethyl-3-(3-dimethylaminopropyl)carbodiimide (EDAC) from Alfa Aesar; *N*-hydroxysuccinimide (NHS) from Fluka; tris (hydroxymethyl)aminomethane buffer (TRIS) from Fisher Bioreagents; ethylenediaminetetraacetic acid (EDTA) from BDG; sodium chloride (NaCl) from Panreac; PVC sheets for the C-SPEs production from Bilcare Research; carbon commercial ink from Electrodag; and silver conductive ink from RS Components Ltd.

Oligonucleotide sequences (anti-microRNA-107 and microRNA-107) were obtained from MeTabion (Planegg, Germany). Anti-microRNA-107 was of DNA nature with an amine 5′-end followed by poly-A spacers; its compete sequence was as follows: 5′-C6 NH_2-AAA AAA AAA ATG ATA GCC CTG TAC AAT GCT GCT-3′. The microRNA-107 was purified by HPLC, with the sequence: 5′-AGC AGC AUU GUA CAG GGC UAU CA-3′.

Solutions were prepared in ultrapure water or ultrapure water treated with DEPC 0.1% for protecting RNA from RNAse degradation. Stock solutions of anti-microRNA-107 (12.6 nM) were prepared in Saline Sodium Phosphate-EDTA Buffer (SSPE) (0.001 M EDTA, 0.149 M NaCl, 0.01 M phosphate buffer, of pH 7.4); stock solutions of the microRNA-107 (36.2 nM) were prepared in Tris-EDTA Buffer (TE, containing 0.01 M Tris, 0.001 M EDTA, and 0.00005 M NaCl, and with pH 7.4). Both solutions were kept frozen (-20 °C).

2.2. Apparatus

The electrochemical data was achieved in the PGSTAT302N, a potentiostat/galvanostat equipment from Metrohm Autolab, controlled

by Nova 1.11 software. The C-SPEs were connected to the potentiostat through a box connector from DropSens. The WE material was analyzed directly by Raman spectroscopy, using a Thermo Scientific, DXR Raman spectrometer, equipped with a 532-nm filter, and by thermogravimetry (TG) using an Hitachi TG/DTA/7200 analyzer.

2.3. Electrochemical assays

Electrochemical assays were performed in equimolar amounts of potassium ferrocyanide and potassium ferricyanide ($[Fe(CN)_6]^{3-/4-}$, 5.0×10^{-3} M) as redox couple, using 0.1 M KCl or TE Buffer (containing 0.01 M Tris, 0.001 M EDTA, and 0.1 M NaCl) as supporting electrolyte, pH of 7.4.

Cyclic voltammograms were obtained by 4 consecutive CVs, for signal stabilization, ranging from −0.7 to +0.7 V for C-SPEs and from −0.7 to +0.9 V for C-SPEs with Ag/AgCl RE, using a scan rate (v) of 50 mV/s. SWV was tested in a potential range of −0.5 to +0.9 V for C-SPEs and −0.3 to +0.9 V for C-SPEs with Ag/AgCl RE, using a frequency of 25 Hz and a step height (amplitude) of 20 mV. EIS assays were achieved in an open circuit potential, with a sinusoidal potential perturbation of 0.01 V amplitude and 50 frequencies, over 0,1 to 100,000 Hz frequency range. All measurements were made at room temperature. Between measurements and incubations, the electrodes were thoroughly rinsed in ultrapure water and softly dried under flowing nitrogen gas.

The chemical modifications in each electrode was followed by checking the variations in the peak current intensity of the anodic (Ip_a) and cathodic (Ip_c) processes, peak potential of the anodic (Ep_a) and cathodic (Ep_c) processes and peak-to-peak separation (ΔEp) from CV; Ip_a and Ep_a from SWV; and charge transfer resistance (R_{ct}) from EIS, for the $[Fe(CN)_6]^{3-/4-}$ redox couple. The Randles circuit with the Warburg element (diffusion, W) was considered in EIS (Fig. S1).

2.4. Surface and materials characterization

Raman spectra were recorded for C-SPEs using a 10× objective and a laser power of 4 mW, with a 50 μm pinhole aperture. Photobleaching was set to 10 min. TG analysis was made with a heating rate of 5 °C/s, from +30 to +1000 °C, under a nitrogen atmosphere at 200 mL/min.

2.5. Fabrication of the C-SPEs

The SPEs, used in this work were assembled by applying a commercial carbon ink on a PVC substrate (Fig. 1A, step 1). The ink was applied (Fig. 1A, step 2) with a spatula until 4 layers of ink had been achieved; each layer was dried in an oven, at 60 °C, for 30 min. Deformation of the substrate took place at temperatures above 60 °C, so this was the maximum temperature that could be employed for curing the ink. After the curing step, the mold mask was removed (Fig. 1A, step 3), a protective layer was applied to insulate the conductive track (Fig. 1A, step 4) and finally, the electrodes were cut from the printed PVC sheet. The resulting electrodes are based in a 3-electrode conventional configuration, consisting in a round shaped WE, with 3-mm diameter, surrounded by a partial circle of a CE and RE (Fig. 1C).

For comparison purposes, C-SPEs with a RE of Ag/AgCl were also prepared. In this case, 1 layer of silver ink was casted in the track of the RE over the previous three carbon electrode system, and let dry at room temperature (Fig. 1B). After this, the silver RE was incubated in iron (III) chloride, 5.0×10^{-3} M, overnight.

Before use, the electrodes were subjected to 40 consecutive CVs, between −2.0 and +2.0 V at a scan rate of 100 mV/s, in KCl 0.1 M [23]. Anticipating the intended application, the WE was also modified with MWNCT-COOH, dispersed by sonication for 1 h, in DMF (1 mg/mL). A volume of 1.5 μL of this suspension was drop-casted on the WE area, and the solvent was dried in the oven, for 10 min, at 60 °C. This step was repeated 3-times.

2.6. Assembling of the sensing element

The sensing layer for microRNA-107 was produced by modifying the carboxylic functions (of the MWCNT-COOH) with EDAC/NHS, prepared in HEPES buffer. A solution of pre-heated (90 °C) anti-microRNA-107 (9,45 μM, in SSPE buffer) was then incubated on the surface for covalent binding of the amine group. Non-specific binding was blocked by incubating L-asparagine.

The calibration of the biosensor was made by incubating increasing microRNA-107 concentrations (from 1.0×10^{-12} up to 1.0×10^{-6} M, in Tris-EDTA buffer or human urine) at the WE, for a given period, followed by reading of the iron redox probe(5 mM of $[Fe(CN)_6]^{3-/4-}$).

3. Results and discussion

3.1. Number of ink layers

The number of ink layers casted on the substrate is a key element in the production of SPEs of good electrical properties. The minimum number of layers yielding good conductivity in the electrical tracks and electrode areas, with a minimum amount of material, should be identified first. One to four ink layers were compare herein. The effect of ink layers upon the electrical response was followed by CV and

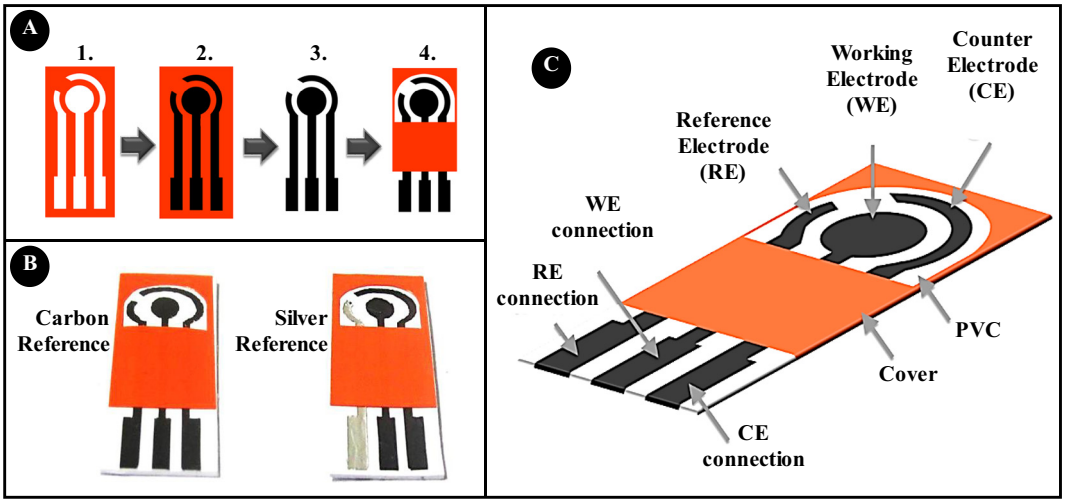

Fig. 1. Schematic representation of the development steps of the C-SPEs production (A), a picture with the real electrodes having different REs (B); and the identification of all components (C).

Nyquist plots in EIS of the standard iron redox probe, covering the three carbon electrodes. Overall, a significant increase in the *Ip* values of the iron redox probe was evidenced when the number of layers changed from 1 to 2 (Fig. S2-A). The *ΔEp* was also narrower with the increasing number of casted layers, being the best values achieved for 4-layer deposition (Fig. S2-A). In EIS, the R_{ct} also decreased along the increasing number of ink layers up to 3, yielding a little R_{ct} increase in the 4th layer deposition (Fig. S2-B). Combining the previous results and considering the lowest *ΔEp*, four ink layers were selected for further studies.

3.2. Surface pre-treatment

It is a regular procedure to pre-treat any electrode surface, to improve the electrode performance and to find reproducible and reliable measurements. Such pre-treating stage is fundamental, as it improves the activity of the electrode [7,9] by removing contaminants and increasing the roughness and the number of reactive sites at the electrode surface. There are numerous physical or chemical pre-treating stages that may be selected for this purpose. However, the most convenient pre-treating approach in an electrochemical-method is to use an electrochemically-based procedure. Herein, the electrode surfaces were subject to consecutive CVs along a wide potential window, in 0.1 M KCl. Electrochemical data was registered after 4 series of 10 consecutive CVs, between 10 and 40 cycles, and the corresponding data is shown in table S1 and Fig. 2.

In general, the increasing number of pre-treatment cycles lead to increasing currents, as evidenced by the consecutive CV scanning. The current detected by the end of each 10 cycling periods is evidenced in the inset of Fig. 2A. This behavior was consistent with that obtained by direct reading of an iron standard redox probe: in CV, the *Ip* values increased significantly after each 10 cycles pre-treating period and the *ΔEp* decreased (Fig. 2B); in EIS, the R_{ct} decreased as the number of pre-treating cycles increased (Fig. 2C).

The raw data of the electrochemical results before treatment and after the 4th cleaning cycle is presented table S1. This data highlighted the poor response of the C-SPEs before pre-treatment, with a large *ΔEp* and thereby a slow-electron transfer rate. After pre-treating, the *Ip* values almost doubled and the observed *ΔEp* corresponding to about 25% of the pristine electrode. Moreover, the ratio of the anodic to cathodic peak (Ip_a/Ip_c) was nearly 1.0, indicating a faster electron transfer rate and evidencing electrochemical reversibility. Besides, the final *ΔEp* suggests the presence of a quasi-reversible system, because all the values are superior of 59/*n* mV (at 25 °C), which is considered the *ΔEp* theoretical value for an ideal electron transfer [24].

Also, we found that after this pre-treatment step, the electrodes are very reproducible. Fig. S3 shows the CV of ten different electrodes, pre-treated and measured in different days. The average and standard deviation were calculated from Ip_a value and were 9.16×10^{-2} mA and 7.62 $\times 10^{-4}$ mA, respectively, showing a low difference between the currents and high inter-electrodes reproducibility.

Overall, the difference between untreated and pre-treated electrodes (Fig. 2B and C and Table S1) was huge, supporting the need for this procedure. The results also pointed out that in the 4th cycle the electrical changes also tended for a stabilization, and therefore a total of 40 CV cycles was implemented before any electrochemical measurement with the C-SPEs. Moreover, the electrochemical results confirmed that the performance of C-SPEs was greatly enhanced by applying the described pre-treatment. It is important to highlight that this is a common need in commercial electrodes, where a pre-treating stage is always applied (which may be different from this one, and depends of the working electrode composition and the commercial brand) if one aims to ensure its stability and reproducibility.

3.3. Supporting electrolytes

The response of the electrodes against different electrolyte supports was tested next. For this purpose, CV of the C-SPEs was recorded in 5.0×10^{-3} M $[Fe(CN)_6]^{3-/4-}$, in different supporting electrolytes (PBS, KCl, KNO_3 and $LiClO_4$, 0.1 M). This study was also made with different scan-rates (10, 25, 50, 100, 150, 200 and 250 mV/s), to calculate the charge-transfer coefficient (α) by means of the Laviron equation (Eq. (1)) [25]. In this, δ_{pa} and δ_{pc} are the anodic and cathodic slopes of linear plots of Ip_a and Ip_c (current of anodic and cathodic peaks, respectively) versus log (*v*, *scan-rate*).

$$\alpha = \frac{\delta pa}{\delta pa - \delta pc} \tag{1}$$

Once the charge-transfer coefficient, α, is known, the electron transfer rate constant (K_s) of the C-SPEs surface can also be calculated by means of Eq. (2) [25]. In this, α was the charge-transfer coefficient, *R* the thermodynamic gas constant [8.314 *J*/(K × mol)], *T* is the temperature (298 K), *n* is the number of electrons transferred in the electrochemical reaction, *F* is the Faraday constant (96,500C/mol), *v* is the scan rate (V/s) and *ΔEp* is the potential difference between the anodic and cathodic peaks.

$$\log(Ks) = \alpha \ \log(1-\alpha) + (1-\alpha) \ \log \alpha - \log\left(\frac{RT}{nFv}\right) - \alpha(1-\alpha) \times \left(\frac{nF\Delta Ep}{2.3RT}\right) \tag{2}$$

The obtained results have been indicated in table S2. From all supporting electrolytes tested, the one showing simultaneously the highest *Ip* values, *Ipa*/*Ipc* close to 1, the lowest ΔE_p and also the highest *Ks* were KCl and KNO_3, thereby indicating faster electron transfer. Comparing these two electrolytes, KCl was the one with the highest *Ks*, being

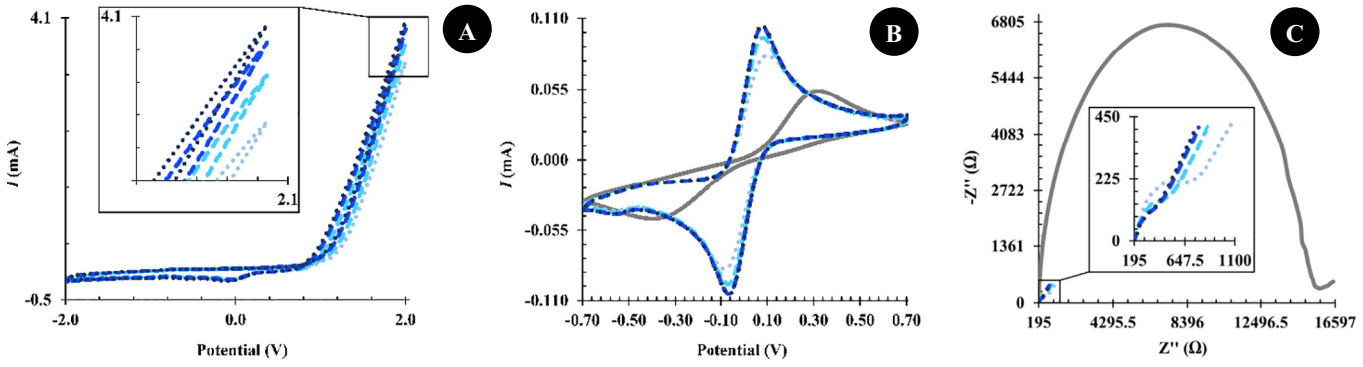

Fig. 2. CV (A) of 10th (•••), 20th (– – –), 30th (– – –) and 40th (•••) cycles of pre-treatment, in 0.1 M KCl. CV (B), and Nyquist impedance (C) plots of the homemade C-SPEs before (—) and after 10 (•••), 20 (– – –), 30 (– – –) and 40 (•••) cycles of pre-treatment in $[Fe(CN)6]^{3-/4-}$, 5.0×10^{-3} M in 0.1 M KCl, at a *v* of 50 mV/s.

therefore selected as supporting electrolyte for $[Fe(CN)_6]^{3-/4-}$ in subsequent experiments.

The effect of scan-rate on the CV of pre-treated C-SPEs, in 5.0×10^{-3} M $[Fe(CN)_6]^{3-/4-}$, prepared in KCl 0.1 M, is made visible in Fig. 3. It was evident that when the scan rate increased, booth Ip_a and Ip_c improved significantly and proportionally. Also, the Ep_a shifted to more positive potentials, while Ep_c moved to more negative values, which is typical of a quasi-reversible electrochemical reaction process [25].

3.4. Surface modification

The modification of the surface is a well-known requirement to assembly almost any biosensor. Such modification shall ensure the presence of a proper functionality at the outer surface, so that binding of the intended biomolecules is made possible. It is also common that such modification occurs with composite materials of highly conductive nanostructures. Examples of these include graphene or carbon nanotubes. Having in mind that the proof-of-concept of these homemade C-SPEs would involve an amine-terminated microRNA, the modification used herein consisted of casting MWCNTs-COOH on the carbon ink. The MWCNTs display high conductivity features and are stably attached to a carbon support through π–π interactions between aromatic rings. After activation by carbodiimide chemistry, the carboxylic acid functions can react (easily) with amines to produce imine derivatives.

As may be seen in Fig. 4 and Table S1, the drop-casting of MWCNTs-COOH hindered the electrical properties of the WE. This was evidenced in all electrochemical techniques employed along this work and most probably reflecting two opposing events: (1) the use of MWCNTs would naturally enhance the electrical features of the WE, due to their extraordinary electrical features out coming from sp^2 carbon hybridization; (2) but the use of carboxylated MWCNTs would disturb the special electrical features of the MWCNTs alone, for destroying partially the sp^2 carbons and introducing sp^3 hybridized atoms that block electron movement.

Moreover, the MWCNTs-COOH were dispersed in DMF; this solvent could also have interacted with the underlying carbon ink or the PVC substrate of the C-SPEs (several solvents were tested for this purpose, but only DMF yielded a stable suspension of MWCNTs-COOH). A suspension of about 1 mg MWCNTs-COOH/1 mL DMF is enough to proceed with the modification of at least 200C-SPEs. Overall, this was a cheap way to add carboxylic groups to the carbon electrode surface and a low cost post-production procedure.

3.5. Carbon versus silver reference electrode

The most common REs in solid-state SPEs are silver (Ag) or silver/silver chloride (Ag/AgCl), used without any coating layer [26]. These Ag or Ag/AgCl electrodes act as pseudo-references, as thermodynamic equilibrium does exist in these. The main concern regarding these pseudo-REs is to achieve good reproducibility within the same batch of devices, intended for disposable applications. The stability of such electrodes in time is hardly a problem, although it may be affected by species in solution that co-precipitate with the cationic metal species (with special concern for chloride, in the case of Ag/AgCl). Although polarization of the RE may be a problem, in a three-electrode system the change of the potential (polarization) of the reference electrode usually causes no problem, since the current flowing between the WE and the RE is typically very small.

Herein, an alternative to the conventional Ag/AgCl is proposed. The RE is made with the same carbon ink used to create RE and CE. For comparison purposes, SPEs with both carbon and Ag/AgCl REs have been prepared, evaluated and compared. The electrochemical plots generated by this study are shown in Fig. S4. The electrochemical data extracted from these results was detailed in table S1.

Regarding the potential values, the results pointed out a shift in the voltammograms generated by different REs: higher potential values for the silver reference. The ΔEp values between cathodic and anodic peaks are similar for SPEs with a different RE system, when these are evaluated under the same conditions. It seems therefore that there is no tendency for widening or narrowing the potential window under work.

Regarding the Ip, a significant difference was observed between the SPEs prepared with different REs. Before and after pre-treating, the carbon RE yielded the best electrochemical performance, but after casting MWCNTs-COOH such difference became negligible. There is indeed no explanation for such behavior, although this was a consistent and repeatable observation.

To understand and support such behavior, further electrochemical data was extracted from the results obtained with the two different REs. Moreover, the electroactive area (A_e) was also calculated, by applying the Randles-Sevcik equation for quasi-reversible electron transfer process (eq. 3). In this, i_p is the peak current intensity (A), n is the number of electrons transferred in the electrochemical reaction, A is the electrode surface area (cm^2), C is the concentration of the analyte (mol/cm^3) and D is the diffusion coefficient (cm^2/s), and v is the scan rate (V/s). To calculate A_e, I_p was plotted against the square root of the scan rate [24,26] and its linear trend used.

$$i_p = \left(2.65 \times 10^5\right) n^{3/2} A C D^{1/2} v^{1/2} \quad (3)$$

The electrochemical data obtained from this study is indicated in table S3. In general, results pointed out that the C-SPEs with carbon ink as RE displayed higher Ks values in all the production stages, in

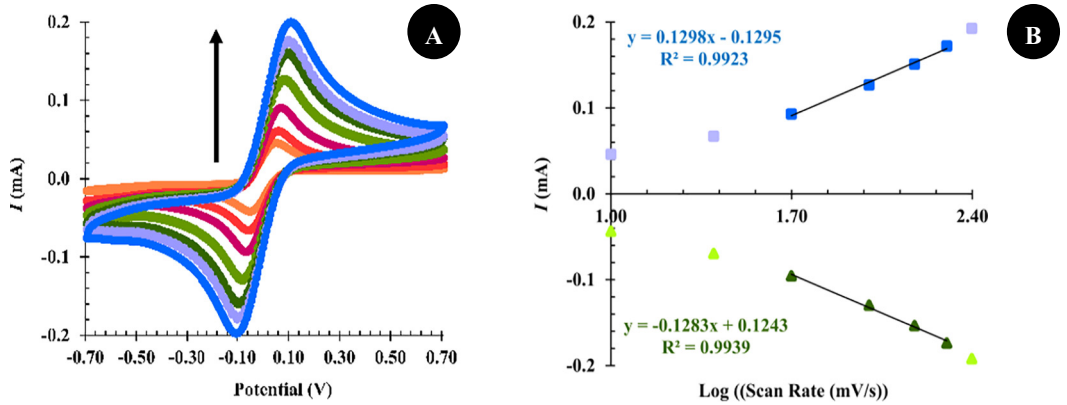

Fig. 3. CVs (a) of C-SPEs in 5.0×10^{-3} M $[Fe(CN)6]^{3-/4-}$, prepared in 0.1 M KCl, with a scan rate of 10 (—), 25 (—), 50 (—), 100 (—), 150 (—), 200 (—) and 250 (—) V/s (from inner to outer) and respective plots (b) of anodic (linear, ■, and nonlinear, ■, range) and cathodic (linear, ▲, and nonlinear, ▲, range) peak currents versus log(v).

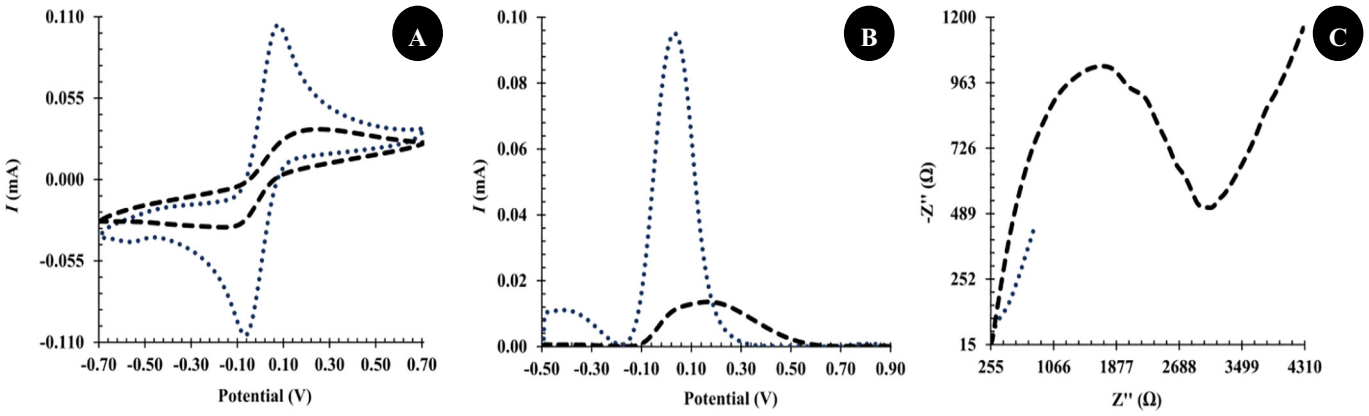

Fig. 4. CV (A), SWV (B) and Nyquist impedance (C) plots of the homemade C-SPEs after pre-treatment (•••) and after drop-casting of the MWCNTs-COOH (– – –), in 5.0×10^{-3} M $[Fe(CN)6]^{3-/4-}$, prepared in 0.1 M KCl, with a scan rate of 50 mV/s.

comparison to the ones with Ag/AgCl RE. The charge-transfer coefficient, α, was similar between the different SPEs electrodes.

The A_e was similar between the two homemade devices (~0.055 cm^2) before the electrochemical pre-treating stage, just as expected (Table S3). After pre-treating, the A_e of the homemade C-SPE with a carbon RE almost doubled (0.114 cm^2), and became much larger than the A_e of the SPEs holding an Ag/AgCl RE (0.083 cm^2). In practice, these values were 1.61 and 1.18× larger than the physical area with which the WEs were prepared (A_g, 0.07065 cm^2), and indicates that a significant amount of carbon particles became exposed at the electrode surface after cleaning, with this effect occurring in a higher extent when the RE was made of carbon. Such differences were probably correlated with the fact that the same potential window in the pre-treating stage did not correspond to the same potential values applied over each WE surface. Thus, care must be taken when selecting the potential window to carry out any electrochemical cleaning approach.

Moreover, the addition of MWCNTs-COOH to the surface yielded SPEs with similar electrochemical features, regardless the material in the RE. The A_e of the C-SPEs with a carbon reference became smaller after casting MWCNTs-COOH on the surface (from 0.114 down to 0.042 cm^2), while a little decrease was observed for the SPEs with a silver RE (from 0.083 to 0.063 cm^2). Considering that the addition of MWCNTs-COOH to the WE surface decreased the electrochemical performance of the device, it seems that a more effective binding to carboxylated material was achieved when the reference was made of carbon, which in turn could have been a consequence of a more effective pre-treating stage on these electrodes.

Overall, and interestingly, the C-SPEs having carbon ink as RE seemed to have a better electrochemical performance than the ones prepared with a silver-based RE. In addition, no issues may be raised regarding the chemical stability of these carbon REs, because these electrodes only contact with the iron redox standard probe. Both calibrating solutions and samples are incubated only on the WE area.

3.6. Characterization of the electrode materials

The materials composing the WE were characterized by Raman spectroscopy and TG. These techniques are complementary and provide valuable information regarding the chemical composition, analyzing directly the material or the electrode surface.

Raman spectroscopy was used to compare the carbon material in the WE, at the different stages of its construction. As expected, all Raman spectra (Fig. S5) showed three prominent peaks [27]: the D band (related with the structural disorder), the G band (linked with the tangential stretching mode of the C═C) and the 2D band (which is a shoulder of the G band at higher frequencies). The Raman shift and intensity of these peaks are indicated in Table S4. In general, the peak positions and intensities were similar before and after treatment. The evident change introduced herein came from the introduction of the MWCNTs-COOH. The Raman shift of the G band was $+7.28$ cm^{-1} while D and 2D bands shifted -4.61 and $+3.79$ cm^{-1}, respectively. The ratio between the intensity of the peaks of the G and D bands (I_G/I_D) suffered a significant decrease after drop-casting MWCNTs-COOH (from 1.28 down to 0.82), signaling the increment of defect sites on the electrode surface and thereby confirming a successful immobilization of the carboxylated nanotubes.

In general, thermograms provide information about the stability of the material against temperature, by indicating the temperature at which the decomposition of materials started; the oxidation temperature; the residual mass [28], among others. The thermograms in Fig. S6 display the curves of weight loss against temperature of carbon materials employed in the fabrication of the C-SPEs. The carbon ink shows 3 stages of decomposition, centering the oxidation peaks at 115, 260 and 420 °C and yielding a total weight loss of 30.5%. From ambient temperature, up to 60 °C there was no significant mass change, indicating that the material was stable within the temperature range (the range used to assemble the C-SPEs).

Regarding the MWCNT-COOH, it is well-known that MWCNTs display high degree of thermal stability and that TG is used to quantify their purity and degree of functionalization [29,30]. Herein, the thermogram recorded relates to the MWCNTs-COOH dispersed in DMF. As expected [30], a continuous weight loss was observed, with a kinetic change at about ~300 °C, until the total elimination of the material. Considering that the nanomaterial was heated under nitrogen atmosphere, its decomposition is expected to release CO_2 (broken C−C bonds linking the carboxylic group to the MWCNT nanostructure) and CH_4. Before 1000 °C, all material was completely lost.

3.7. Application to microRNA-107 detection

The biosensor was assembled according to the schematic representation in Fig. 5A. It started by activating the –COOH groups exposed at the surface via carbodiimide chemistry, aiming to bind directly the anti-microRNA-107. As expected, the addition of the complementary oligonucleotide probe decreased the current generated by the iron redox probe, which was coupled to an increase in the R_{ct} (Fig. 5B to D). The —COOH reaming active after this, were deactivated by reaction with L-asparagine; this event contributed to an additional *Ip* decrease (in CV and SWV) and R_{ct}, in EIS. Overall, these results confirmed a successful immobilization of the anti-microRNA-107 and subsequent blocking of non-specific bindings by L-asparagine.

The resulting biosensor was stabilized in buffer (black line in Fig. 6) and then incubated in the lowest concentration of microRNA-107 tested herein, equal to 1.0 pM. After incubation, the 3-electrode system was washed and the electrochemical signals of the iron standard probe recorded. The hybridization of microRNA-107 was detected by an additional decrease in the current signals and an increase in the R_{ct}. This procedure was repeated continuously, up to the maximum concentration tested, 1.0 μM of microRNA-107. Overall, the data obtained showed linear trends in SWV and EIS against logarithm concentration, corresponding to Current *I*p (mA) $= -6.0 \times 10^{-4} \times$ log[microRNA, mol/L] $- 9.0 \times 10^{-4}$ (R-squared of 0.9924) and R_{ct} (Ω, open circuit potential) $= 1589.4 \times$ log [microRNA, mol/L] + 26,802 (R-squared of 0.9876), respectively. The linear behavior was observed between 1.0 pM and 1.0 μM, all concentration values tested herein.

This linear behavior agreed with the information reported in Bode's plot, in Fig. 6D. In this, the linear behavior was Z (Ω) $= 993.63 \times$ log[microRNA, mol/L] + 18,934 (R-squared of 0.9814), when reflecting the R_{ct} in the modulus plot, and Degree (°) $= 1.4908 \times$ log[microRNA, mol/L] + 51.896 (R-squared of 0.9953), when reflecting the R_{ct} in the phase plot.

Overall, these are promising results, considering that a homemade three carbon electrode system is well-suited for surface modification, which in turn can produce a quantitative response against a given analyte, even within the pM range.

3.8. Practical application in urine samples

To test a practical application of the biosensor, a calibration in human samples were performed. The obtained data is presented in Fig. 7. For this purpose, the biosensor was stabilized with blank human urine and then incubated with miRNA-107 concentrations from 1.0 pM up to 1.0 μM. *Ipa* current of SWV against logarithmic concentration was linear in a wide range, from 1.0 pM to 0.1 μM, with the regression equation of Current Ip (mA) $= -5.0 \times 10^{-4} \times$ log[microRNA, mol/L] $- 5.3 \times 10^{-3}$ (R-squared of 0.9948). For R_{ct} values against logarithmic concentration, the linear regression equation of the assay was R_{ct} (Ω, open circuit potential) $= 1098.4 \times$ log [microRNA, mol/L] + 27,739 (R-squared of 0.9935), having a linear response between 10 pM up to 1 μM. The detection limits, calculated considering the slope of the linear portion of the calibration curve was, <1.0 pM and 7.08 pM for SWV and EIS, respectively.

4. Conclusions

In this work, the best conditions to produce homemade C-SPEs with a 3 carbon electrode system were identified. The pre-treating stages of the WE surface exerted a great influence upon the electrochemical performance of the final device. Care must be taken at the electrochemical cleaning stage, because little alterations in the potential range applied (out coming herein from the RE) may yield different electrical outputs. The carbon WE is also suited for chemical modification, in agreement with the intended application of the device.

Comparing to other electrochemical biosensors for microRNAs in the literature based on SPEs (Table 1), some advantages may he highlighted. Most of reported works used Au-SPEs, which have a cost and performance that is not comparable with carbon electrodes. Although the LOD reported herein is typically higher than the ones achieved in the reported works, it is worthy to highlight the advantage of simplicity of our assay as compared to the other reported assays and the fact that all the SPEs-based biosensors reported so far have a silver pseudo-reference electrode while ours is the only one made by carbon.

Overall, a way of producing disposable and flexible homemade C-SPEs is presented herein, highlighting that only simple procedures are employed and the electrical performance is comparable to similar commercial devices, used for other purposes. The devices are promising,

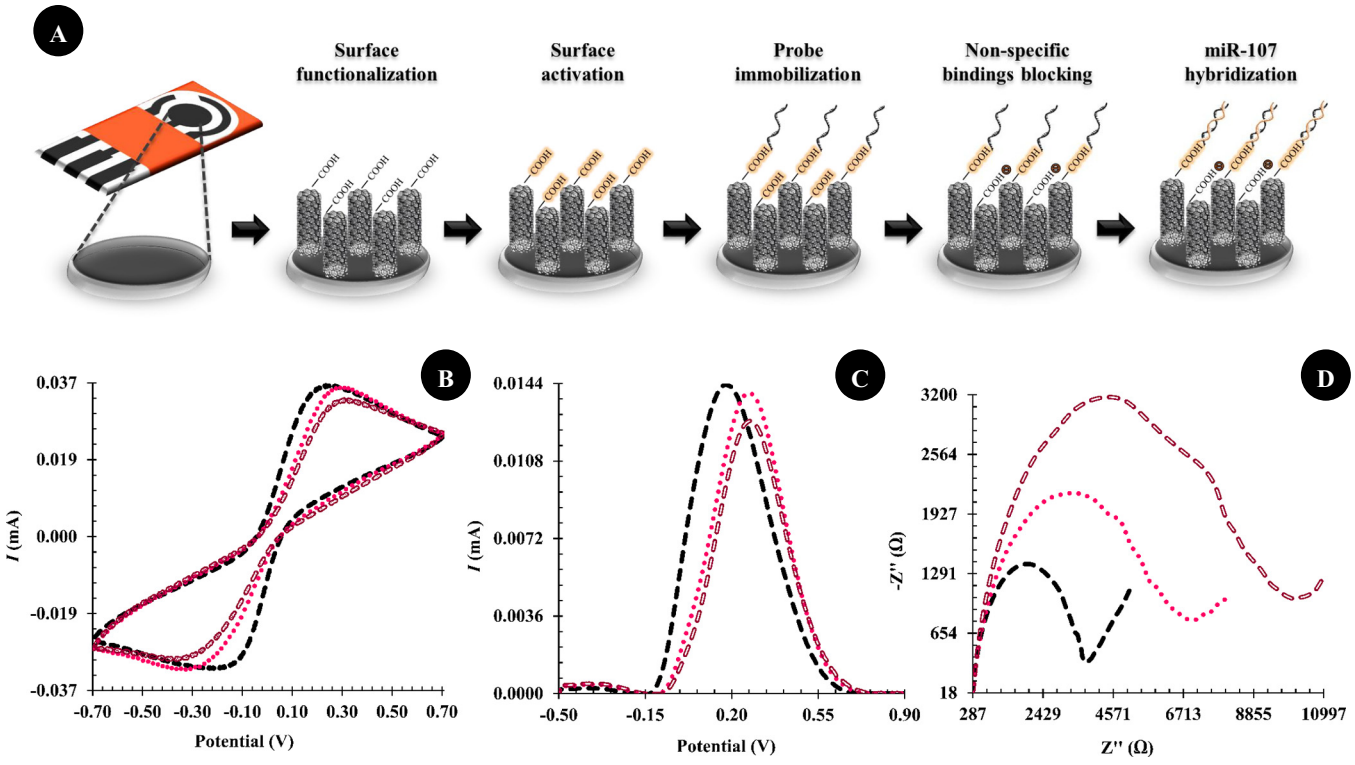

Fig. 5. Schematic representation of the assembly of the biosensor (A) and its electrochemically generated signals by CV (B), SWV (C) and EIS (D) after MWCNTs-COOH deposition (– – –), anti-miRNA binding (•••), and L-asparagine binding (– – –).

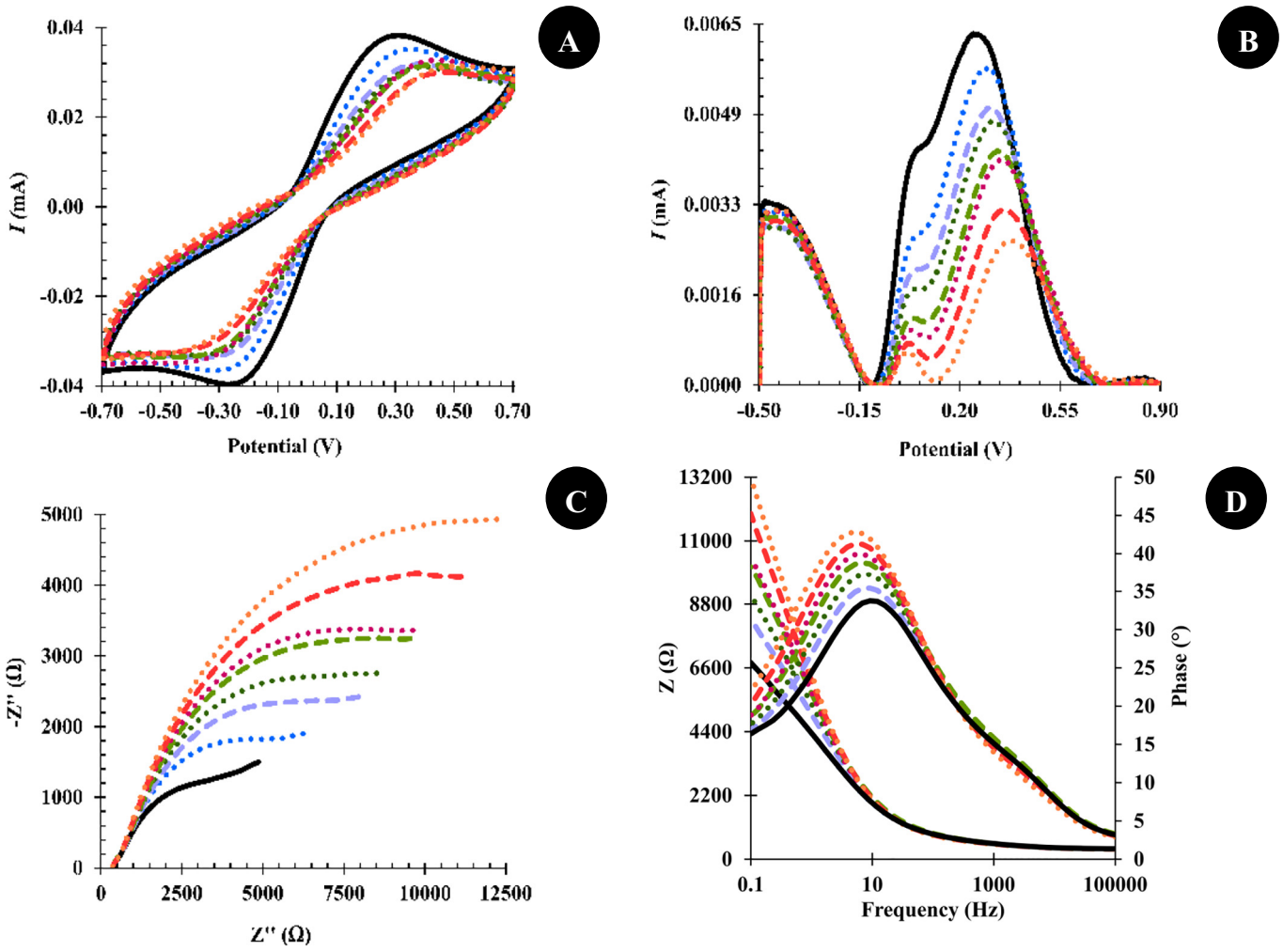

Fig. 6. CV (A), SWV (B), Nyquist (C) and Bode's plot (D) of the biosensor calibration in buffer. TE buffer stabilization (▬) and incubation with microRNA-107 increasing concentrations, of 1.0×10^{-12} M (•••), 1.0×10^{-11} M (– – –), 1.0×10^{-10} M (•••), 1.0×10^{-9} M (– – –), 1.0×10^{-8} M (•••), 1.0×10^{-7} M (– – –) and 1.0×10^{-6} M (•••).

working well enough to become a low-cost disposable device in disease screening. Additional tests are most certainly necessary prior to any intended commercial utilization of the described procedure.

Moreover, the proof-of-concept performed by using the developed electrodes in a biosensor shows that these are suitable for miRNA-107 detection, in a low-cost and simple assay.

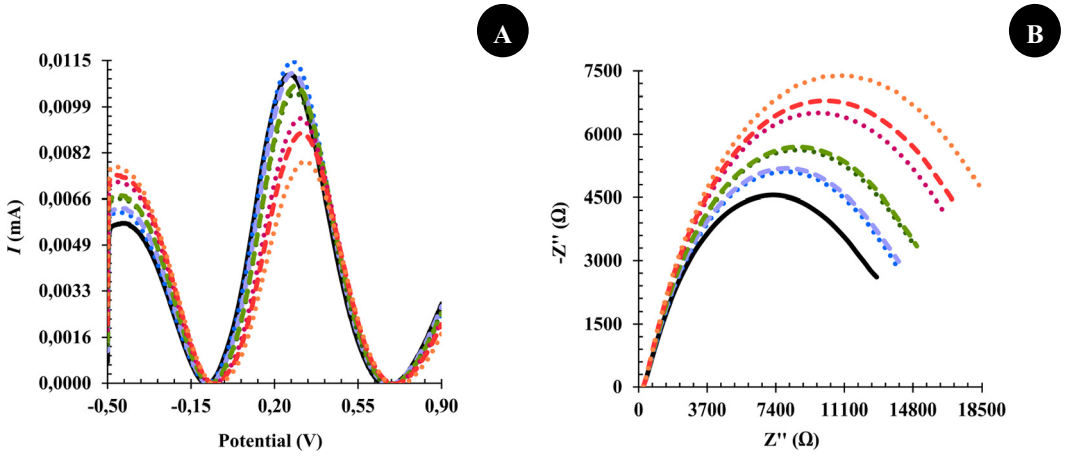

Fig. 7. SWV (A) and Nyquist plot (B) of the biosensor calibration in urine. Urine stabilization (▬) and incubation with microRNA-107 increasing concentrations, of 1.0×10^{-12} M (•••), 1.0×10^{-11} M (– – –), 1.0×10^{-10} M (•••), 1.0×10^{-9} M (– – –), 1.0×10^{-8} M (•••), 1.0×10^{-7} M (– – –) and 1.0×10^{-6} M (•••).

Table 1
Recent works reporting electrochemical biosensors based on screen printed electrodes for microRNAs detection.

miRNA	Support	RE	Technique	Methodology	LOD (mol/L)	Linear response (mol/L)	Reference
106a	SPCE	Silver	DPV	Au-magnetic-streptavidin-labeled nanoparticles decorated with ss-biotin-labeled CP 1 hybridizes with the target and are captured by a ss-biotin-labeled CP 2, immobilized onto the streptavidin-labeled SPE	3×10^{-16} M	1×10^{-15} to 1×10^{-9} M	[31]
122	SPCE	Silver	DPV	Biotinylated DNA CP immobilized on streptavidin-coated paramagnetic beads are incubated with the biotinylated target. The hybrids are labeled with a streptavidin–AP, magnetically entrapped onto the SPE and exposed to enzymatic substrate	7×10^{-12} M	0 to 1×10^{-9} M	[32]
21, 32 and 122	GNPs-SPCE	Silver	SWV and EIS	Three sensing modalities (direct hybridization with the target miRNA, p19 protein binding, and protein displacement)	5×10^{-18} M	1×10^{-17} to 1×10^{-6} M	[33]
34a	CNF-SPGE	Silver	DPV	An amino linked inosine substituted DNA CP immobilized onto the SPE hybridizes with the target	1.51×10^{-6} M	3.45×10^{-6} to 1.38×10^{-5} M	[34]
141	Au-SPE/RGO/MWCNT	Silver	SWV	A CP immobilized onto the SPE hybridizes with the target and an antibody selectively binds to the hybrid. A secondary antibody conjugated to HRP oxidizes hydroquinone into benzoquinone which is electroreducted into hydroquinone at the SPE	1×10^{-14} M	1×10^{-14} to 1×10^{-10} M	[35]
21	Au-SPE	Silver	DPV	Two auxiliary probes self-assembly to form DNA concatamers. In the presence of the target, DNA concatamers hybridize with unfolded CP, immobilized onto the SPEs	1×10^{-16} M	1×10^{-16} to 1×10^{-10} M	[36]
155	Au-SPE	Silver	SWV and EIS	A thiol linked CP immobilized onto the SPE hybridizes with the target	5.7×10^{-18} M	1×10^{-17} to 1×10^{-9} M	[21]
107	Au-SPE	Silver	DPV	Streptavidin-coated magnetic beads coupled with CP bind to the target. The hybridized target is magnetically purified, released from CPs and modified with poly(A) extension prior to adsorption onto the SPE	1×10^{-14} M	5×10^{-15} to 5×10^{-12} M	[37]
107	Au-SPE	Silver	CC	Streptavidin-labeled dyanabeads modified with a biotin-labeled CP bind to target, purifying and isolating it from the sample. The target directly adsorbs on the Au-NPFe_2O_3NC, immobilized on the SPE. Ru$[(NH_3)_6]^{3+}$ bind to the target and the signal is amplified by its reduction by Fe$[(CN)_6]^{3-}$	1×10^{-16} M	1×10^{-16} to 1×10^{-9} M	[38]
107	SPCE	Carbon	SWV EIS	An amino linked DNA CP immobilized onto the SPCE hybridizes with the target	$<1 \times 10^{-12}$ M 7.08×10^{-12} M	1×10^{-12} M to 1×10^{-6} M 1×10^{-11} M to 1×10^{-6} M	This work

AP (alkaline phosphatase), Au-NPFe_2O_3NC (gold-loaded nanoporous superparamagnetic iron oxide nanocubes), Au-SPE (Screen Printed Gold Electrode), CNF (Carbon Nanofiber), CC (Chronocoulomery), CP (capture probe), DPV (Differential Pulse Voltammetry), EIS (Electrochemical Impedance Spectroscopy), GNPs (Gold Nano-Particles), HRP (horseradish peroxidase), SPE (Screen Printed Electrode), miRNA (micro-RNA), MWCNTs (Multi-Walled Carbon Nanotubes), RE (Reference Electrode), RGO (Reduced Graphene Oxide), Ru$[(NH_3)_6]^{3+}$ (Ruthenium heaxaammine III chloride), SPCE (Screen Printed Carbon Electrode), SPGE (Screen Printed Graphite Electrode), ss (Single Stranded), SWV (Square Wave Voltammetry).

Acknowledgements

Authors acknowledge funding from Fundação para a Ciência e Tecnologia, I.P., and European funding to FEDER (European Funding or Regional Development, via COMPETE2020 – POCI, operational program for internationalization and competitiveness, through the project PTDC/AAG-TEC/5400/2014, POCI-01-0145-FEDER-016637). FTCM acknowledges Fundação para a Ciência e a Tecnologia (Post-Doc grant reference SFRH/BPD/97891/2013).

References

[1] X. Qin, S. Xu, L. Deng, R. Huang, X. Zhang, Photocatalytic electrosensor for label-free and ultrasensitive detection of BRCA1 gene, Biosens. Bioelectron. 85 (Supplement C) (2016) 957–963 2016/11/15/.

[2] H.M. Mohamed, Screen-printed disposable electrodes: Pharmaceutical applications and recent developments, TrAC Trends Anal. Chem. 82 (2016) 1–11 9.

[3] N.J. Ronkainen, H.B. Halsall, W.R. Heineman, Electrochemical biosensors, Chem. Soc. Rev. 39 (5) (2010) 1747–1763 10.1039/B714449K.

[4] F. Wang, S. Hu, Electrochemical sensors based on metal and semiconductor nanoparticles, Microchim. Acta 165 (1) (2009) 1–22 2009/04/01.

[5] T. Gan, S. Hu, Electrochemical sensors based on graphene materials, Microchim. Acta 175 (1) (2011) 1 2011/07/07.

[6] M. Tudorache, C. Bala, Biosensors based on screen-printing technology, and their applications in environmental and food analysis, Anal. Bioanal. Chem. 388 (3) (2007) 565–578.

[7] Z. Taleat, A. Khoshroo, M. Mazloum-Ardakani, Screen-printed electrodes for biosensing: a review (2008–2013), Microchim. Acta 181 (9) (2014) 865–891 2014/07/01.

[8] A. Hayat, L.J. Marty, Disposable screen printed electrochemical sensors: tools for environmental monitoring, Sensors 14 (6) (2014).

[9] P. Fanjul-Bolado, D. Hernández-Santos, P.J. Lamas-Ardisana, A. Martín-Pernía, A. Costa-García, Electrochemical characterization of screen-printed and conventional carbon paste electrodes, Electrochim. Acta 53 (10) (4/1/2008) 3635–3642.

[10] A.P. Ruas de Souza, C.W. Foster, A.V. Kolliopoulos, M. Bertotti, C.E. Banks, Screen-printed back-to-back electroanalytical sensors: heavy metal ion sensing, Analyst 140 (12) (2015) 4130–4136 10.1039/C5AN00381D.

[11] S.L.R. Gomes-Filho, A.C.M.S. Dias, M.M.S. Silva, B.V.M. Silva, R.F. Dutra, A carbon nanotube-based electrochemical immunosensor for cardiac troponin T, Microchem. J. 109 (Supplement C) (2013/07/01) 10–15.

[12] K. Yamanaka, M.D.C. Vestergaard, E. Tamiya, Printable electrochemical biosensors: a focus on screen-printed electrodes and their application, Sensors 16 (10) (2016) 1761 10/21 07/15/received 09/23/accepted.

[13] J.P. Hart, A. Crew, E. Crouch, K.C. Honeychurch, R.M. Pemberton, Some recent designs and developments of screen-printed carbon electrochemical sensors/biosensors for biomedical, environmental, and industrial analyses, Anal. Lett. 37 (5) (2004/01/01) 789–830.

[14] C. Tortolini, M. Di Fusco, M. Frasconi, G. Favero, F. Mazzei, Laccase–polyazetidine prepolymer–MWCNT integrated system: Biochemical properties and application to analytical determinations in real samples, Microchem. J. 96 (2) (2010/11/01) 301–307.

[15] G.L. Inzelt, A. Scholz, Handbook of Reference Electrodes, 1 ed Springer-Verlag, Berlin Heidelberg, 2013.

[16] V. Dorval, P.T. Nelson, S.S. Hébert, Circulating microRNAs in Alzheimer's disease: the search for novel biomarkers, Front. Mol. Neurosci. 6 (2013).

[17] G.D. Femminella, N. Ferrara, G. Rengo, The emerging role of microRNAs in Alzheimer's disease(in Eng) Front. Physiol. 6 (2015) 40.

[18] P. Leidinger, et al., A blood based 12-miRNA signature of Alzheimer disease patients(in Eng) Genome Biol. 14 (7) (2013) R78.

[19] M. de Planell-Saguer, M.C. Rodicio, Analytical aspects of microRNA in diagnostics: a review, Anal. Chim. Acta 699 (2) (8/12/2011) 134–152.

[20] B.N. Johnson, R. Mutharasan, Biosensor-based microRNA detection: techniques, design, performance, and challenges, Analyst 139 (7) (2014) 1576–1588 10.1039/C3AN01677C.

[21] A.R. Cardoso, F.T.C. Moreira, R. Fernandes, M.G.F. Sales, Novel and simple electrochemical biosensor monitoring attomolar levels of miRNA-155 in breast cancer, Biosens. Bioelectron. 80 (6/15/2016) 621–630.

[22] M. Azimzadeh, M. Rahaie, N. Nasirizadeh, K. Ashtari, H. Naderi-Manesh, An electrochemical nanobiosensor for plasma miRNA-155, based on graphene oxide and gold nanorod, for early detection of breast cancer, Biosens. Bioelectron. 77 (3/15/2016) 99–106.

[23] M.A. Alonso-Lomillo, C. Yardimci, O. Domínguez-Renedo, M.J. Arcos-Martínez, CYP450 2B4 covalently attached to carbon and gold screen printed electrodes by diazonium salt and thiols monolayers, Anal. Chim. Acta 633 (1) (2/2/2009) 51–56.

[24] D. Martín-Yerga, E. Costa Rama, A. Costa García, Electrochemical study and determination of electroactive species with screen-printed electrodes, J. Chem. Educ. 93 (7) (2016/07/12) 1270–1276.

[25] X. Fang, L. Wu, Handbook of Innovative Nanomaterials: From Syntheses to Applications, Pan Stanford, New York, 2012.

[26] D.A.C. Brownson, C.E. Banks, Interpreting electrochemistry, in: C.D.A. Brownson, E.C. Banks (Eds.), The Handbook of Graphene Electrochemistry, Springer London, London 2014, pp. 23–77.

[27] W.M. Silva, et al., Surface properties of oxidized and aminated multi-walled carbon nanotubes, J. Braz. Chem. Soc. 23 (2012) 1078–1086.

[28] J.H. Lehman, M. Terrones, E. Mansfield, K.E. Hurst, V. Meunier, Evaluating the characteristics of multiwall carbon nanotubes, Carbon 49 (8) (7/2011) 2581–2602.

[29] C.A. Dyke, J.M. Tour, Solvent-free functionalization of carbon nanotubes, J. Am. Chem. Soc. 125 (5) (2003/02/01) 1156–1157.

[30] B.V. Farahani, G.R. Behbahani, N. Javadi, Functionalized multi walled carbon nanotubes as a carrier for doxorubicin: drug adsorption study and statistical optimization of drug loading by factorial design methodology, J. Braz. Chem. Soc. 27 (2016) 694–705.

[31] M. Daneshpour, K. Omidfar, H. Ghanbarian, A novel electrochemical nanobiosensor for the ultrasensitive and specific detection of femtomolar-level gastric cancer biomarker miRNA-106a, Beilstein J. Nanotechnol. 7 (2016) 2023–2036 12/19 08/30/received 11/23/accepted.

[32] F. Bettazzi, et al., Electrochemical detection of miRNA-222 by use of a magnetic bead-based bioassay, Anal. Bioanal. Chem. 405 (2) (2013/01/01) 1025–1034.

[33] M. Labib, N. Khan, S. Ghobadloo, J. Cheng, J. Paul Pezacki, M. Berezovski, Three-mode Electrochemical Sensing of Ultralow MicroRNA Levels, 2013.

[34] A. Erdem, E. Eksin, G. Congur, Indicator-free electrochemical biosensor for microRNA detection based on carbon nanofibers modified screen printed electrodes, J. Electroanal. Chem. 755 (Supplement C) (2015/10/15) 167–173.

[35] H.V. Tran, et al., An electrochemical ELISA-like immunosensor for miRNAs detection based on screen-printed gold electrodes modified with reduced graphene oxide and carbon nanotubes, Biosens. Bioelectron. 62 (Supplement C) (2014/12/15) 25–30.

[36] M.N. Sonuç, M.K. Sezgintürk, Ultrasensitive electrochemical detection of cancer associated biomarker HER3 based on anti-HER3 biosensor, Talanta 120 (Supplement C) (2014/03/01) 355–361.

[37] K. Koo, L. Carrascosa, M. Shiddiky, M. Trau, Poly(A) Extensions of miRNAs for Amplification-free Electrochemical Detection on Screen-Printed Gold Electrodes, 2016.

[38] S. Yadav, et al., Gold-loaded nanoporous iron oxide nanocubes: a novel dispersible capture agent for tumor-associated autoantibody analysis in serum, Nanoscale 9 (25) (2017) 8805–8814 10.1039/C7NR03006A.